Morphological evolution of ion-sputtered Pd(001): Temperature effects

T. C. Kim, M. H. Jo, Y. Kim, and D. Y. Noh

Department of Materials Science and Engineering, Gwangju Institute of Science and Technology, Gwangju 500-712, Korea

B. Kahng

School of Physics and Center for Theoretical Physics, Seoul National University, Seoul 151-747, Korea

J.-S. Kim*

Department of Physics, Sook-Myung Women's University, Seoul 140-742, Korea

We have investigated the kinetic effects on the morphological evolution of an Ar^+-ion sputtered Pd(001) by *in situ*, real-time x-ray reflectivity and grazing-incidence small angle x-ray scattering measurements at various substrate temperatures. We find that surface roughness W and its associated growth exponent β increase with T up to a certain temperature T_m. Beyond T_m, however, they decrease with increasing T. For $T < T_m$, surface roughening and coarsening kinetics are mostly driven by the deposition and diffusion of sputter-induced adatoms as reported in molecular beam epitaxial growth. When T is near T_m, however, vacancies rather than adatoms become the dominant surface species. Above T_m, the surface smoothing via adatom detachment and vacancy diffusion across step edges becomes effective.

I. INTRODUCTION

Recently, there has been increasing interest in surface modification by ion sputtering. Fabrications of self-organized ordered nanostructures are demonstrated by simply adjusting physical parameters involved in ion sputtering such as ion beam energy, flux, incidence angle, and substrate temperature.[1–6] Generally, the interplay between surface roughening induced by ion sputtering and smoothing by the diffusion of sputter-induced adatoms and vacancies is considered to play a major role in producing ordered structures on sputtered surface. Although there have been many successful results and hopeful prospects for nanostructure fabrication, the microscopic processes of the morphological evolution of ion-sputtered surfaces have not been fully understood yet.

Numerous continuum models[7–13] and numerical simulations[14–16] have successfully elucidated many features of sputter-eroded surfaces. Despite the notable progress made by such studies based on simplified models, they lack in coherence. This is partly due to the complexity of the sputtering and sputter-induced processes such as erosion dynamics, redeposition, and diffusion kinetics of adatoms as well as vacancies. Another reason lies in the insufficient experimental investigations exposing various aspects and details of sputtered morphology and relevant growth mechanisms. Especially, experimental studies on the effect of diffusion kinetics on morphological evolution[2,14,17–19] are rare due to the technical difficulties involved in sputtering substrate over various surface temperatures, and measuring the modified surface morphology *in situ* and in real time.

We investigate the morphological evolution of Ar^+ sputtered Pd(001) by using *in situ*, real-time x-ray reflectivity (XRR) and grazing-incidence small angle x-ray scattering (GISAXS) at substrate temperatures T, ranging from 306 to 440 K. This work is unique compared with previous experimental works, since we investigate both kinetic rough-

ening and coarsening in real time for an extended period of sputter time that is enough to observe related crossover behavior closely, and for a wide range of T from thermally frozen temperature to the temperature where smoothing kinetics becomes effective. We find that in the temperature regime where the kinetics of sputter-induced adatom governs morphological evolution, the sputtered surface is similarly well described by the model of molecular beam epitaxial (MBE) growth. At high temperatures where the other kinetic processes such as vacancy diffusion and atomic detachment from step edge are dominant, the MBE models do not fully reproduce the features of sputtered surface morphology.

II. EXPERIMENT

Clean Pd(001) surface is obtained by repeated cycles of Ar^+ sputtering around 300 K and annealing at 950 K. The Pd(001) shows an average terrace size of about 1000 Å, estimated by the width of specular x-ray beam. The surface roughness of the sample, defined as the root-mean-square fluctuations of the surface height, is less than 2.5 Å, and the miscut from the surface normal is 0.3° as determined, respectively, by XRR and x-ray diffraction spot profile analysis. All the experiments are performed in an ultrahigh vacuum (UHV) x-ray scattering chamber, the base pressure of which is below 5×10^{-10} Torr.

In order to investigate the evolution of the surface roughness and the coarseness during Ar^+ sputtering, XRR and GISAXS are measured at the beamline 5C2 at the Pohang light source (PLS). For the measurement, a custom-designed UHV chamber mounted on a four-circle diffraction goniometer (2+2 mode) is employed. The incident x-rays are vertically focused by a mirror and monochromatized to a wavelength $\lambda = 1.239$ Å by a double bounce Si(111) monochromator. Both XRR and GISAXS measurements are made
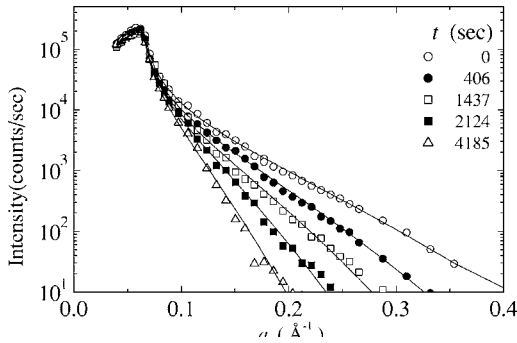
FIG. 1. Specular x-ray reflectivity (symbols) as a function of the out-of-plane momentum transfer q_z for increasing sputtering time t with $\epsilon = 0.5$ keV and $f = 0.5 \times 10^{13}$ ions/cm²/s at 421 K. The solid lines are the theoretical prediction from the Parratt's formula.

in situ and in real time. The acquisition time for each data point is smaller than the overall sputter time by more than an order of magnitude, and the evolution of surface morphology is properly followed by both measurements.

The sample temperature is monitored by both a thermocouple directly attached to the backside of the sample and an optical pyrometer. The sample temperature T was controlled by dc Joule heating through a Ta ledge (purity of 99.999%), attached to the sample. To avoid any artifact due to temperature fluctuations during measurement, we have controlled the sample temperature within ±3 K during the entire measurement.

Sputtering of the Pd(001) surface was carried out with Ar⁺-ion beam incident normal to the sample surface. Ar⁺-ion energy ϵ was 0.5 keV and ion flux, $f = 0.5 \times 10^{13}$ ions/cm²/s. The ion beam was defocused in order to irradiate the sample surface uniformly. To avoid possible contamination of the sample during sputtering, fresh Ar gas (purity of 99.999%) was continuously flown through the chamber under a pressure maintained at 2.0×10^{-5} Torr.

III. RESULTS

In situ, real-time specular XRR measurement is made to investigate the evolution of surface roughness during Ar⁺-ion sputtering. In the Born approximation, the specular XRR decreases as $\sim \exp(-W^2 q_z^2)$ with increasing q_z, where W is surface width or roughness, and q_z is the component of momentum transfer perpendicular to the surface.[20] Figure 1 shows that XRR decreases more sharply as the sputtering proceeds, which indicates that the surface becomes rougher or $W(t)$ increases with increasing t. W is determined by fitting of the experimental XRR curve according to the Parratt formalism.[20,21]

Figure 2(a) summarizes the evolution of $W(t)$ thus obtained as a function of sputtering time t at various sample temperatures T ranging from 306 to 440 K. Ion beam energy ϵ and ion flux f are fixed at 0.5 keV and 0.5×10^{13} ions/cm²/s, respectively. The linear dependence of $W(t)$ on sputtering time t in a double logarithmic scale plot implies a power-law behavior $W(t) \sim t^\beta$, where β is the growth exponent. In between the two temperatures 306 and
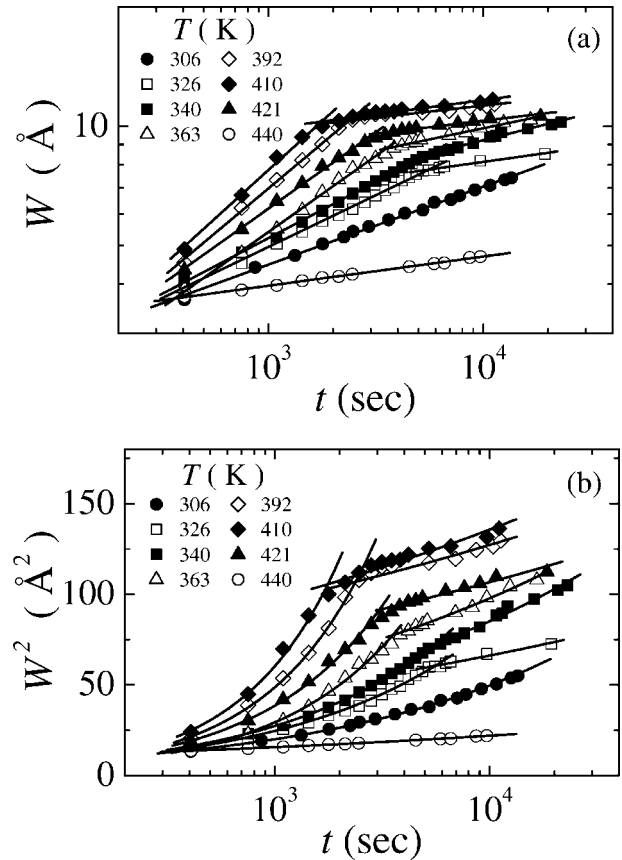

FIG. 2. The surface width or roughness W as a function of sputtering time t for different temperature T (symbols) with $\epsilon = 0.5$ keV and $f = 0.5 \times 10^{13}$ ions/cm²/s. Before t_c, the solid lines represent fitting results by power law, $W(t) \sim t^\beta$ with large β in the range $\beta \approx 0.2 \sim 0.5$. After t_c, nice fit can be made by either (a) small $\beta \approx 0.1$, or (b) $W^2(t) \sim \log t$.

440 K, well defined crossovers are observed in the dynamic scaling behavior of $W(t)$: After the crossover time t_c, $W(t)$ grows much slower than it does before t_c, which is also manifested in small value of $\beta \approx 0.1$.

Each curve in Fig. 3 represents the temperature dependence of W for the respective fixed fluence or sputter time, which is extracted from Fig. 2. We observe reentrant behavior of $W(T)$ for all the fluences: W gradually increases with increasing T from 306 to 410 K. Above 410 K, however, W
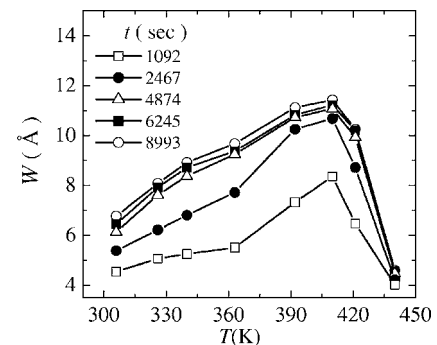

FIG. 3. Surface roughness W as a function of the sample temperature, T, for different Ar⁺-ion fluences.
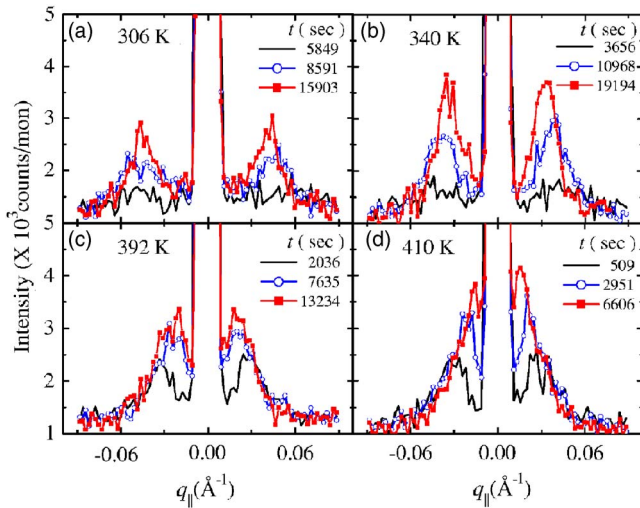
FIG. 4. (Color online) Evolution of grazing-incidence small-angle x-ray scattering (GISAXS) profile. Each scan is made along the [110] direction, $q_\parallel$ through specular rods at q_z=0.1769 Å^{-1}. The profiles are measured during sputtering with ϵ=0.5 keV and f =0.5×10^{13} ions/cm^2/s for different temperatures T (a) 306 K, (b) 340 K, (c) 392 K, and (d) 410 K. For all profiles, the position of the satellite peak shifts to smaller $q_\parallel$ with increasing sputtering time t.

decreases again rapidly. This indicates that initial roughening is followed by smoothing kinetics at elevated temperatures. Such reentrant behavior of $W(T)$ has also been reported for Ag(001).[2,22]

To examine the lateral structure formed during sputtering, transverse scans are made along the in-plane, close-packed [110] direction $q_\parallel$ across the specular rod at q_z=0.1769 Å^{-1} (Fig. 4). We observe a specular peak at the center and two satellite peaks on its sides. It may reflect the formation of a laterally ordered structure and its coarsening during sputter processes. However, such satellite peaks may also originate from facets formed during sputtering. To clarify the origin of the satellite peak, we carried out a series of transverse scans through different q_z's along the specular reflection rod at different T from 306 to 363 K (Fig. 5). The position of satellite peaks stays constant as q_z varies between 0.1327 and 0.2211 Å^{-1}. We, therefore, conclude that the satellite peaks originate from a laterally ordered structure on the sputtered surface, not from facets.

The positions of the satellite peaks in each transverse scan curve are determined by fitting each curve to a model with three simple gaussians and a constant background. Then, the lateral characteristic length ξ is obtained from the separation between two satellite peak positions $\Delta q_\parallel^{peak}$ as ξ=4π/$\Delta q_\parallel^{peak}$. Figure 6 summarizes the temporal evolution of ξ at various substrate temperatures. ξ grows as sputtering proceeds, which means that the coarsening of islands and/or pits proceeds with increasing sputter time t.[23] Above 410 K, ξ becomes so large that the satellite peaks occur too close to the specular peak, and it is impossible to determine ξ. As shown in Fig. 6, $\xi(t)$ is well described by a power law $\xi \sim t^{1/z}$, where $1/z$ is the coarsening exponent. It is noteworthy that ξ does not show any crossover behavior, in contrast to $W(t)$ [Fig. 2(a)].
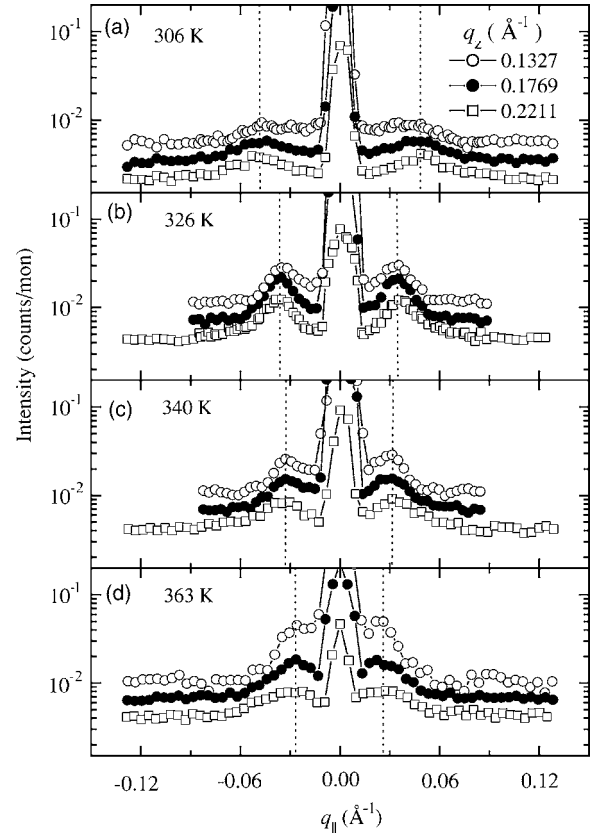

FIG. 5. Transverse scans along [110] through specular rods at various q_z's. Ion fluence is 9.2×10^{16} ions/cm^2 at different T's from 306 to 363 K.

The values of β and $1/z$ are summarized as a function of T in Fig. 7. β before t_c also shows a reentrant bell-shape dependence on T, as is the case for $W(T)$; it increases from 0.20±0.02 to 0.49±0.04 as does T from 306 to 410 K. Above 410 K, however, β rapidly decreases from 0.49±0.04 to 0.07±0.02 at 440 K. After t_c, β becomes very small around 0.1, and shows no regular dependence on T. On the other hand, $1/z$ shows relatively little variation, staying between 0.15 and 0.25, and does not show any crossover behavior.

IV. DISCUSSION

A. Crossover behavior

The roughness evolution shown in Fig. 2(a) exhibits distinguished behaviors before and after t_c, giving very different β's. While the dynamic exponent β, describing the temporal evolution of the surface width, has relatively large value ~0.2–0.5 before t_c, after which β is reduced to β~0.1, irrespective of substrate temperature. Such a small value of β suggests that the surface evolution may belong to the class of the Edwards-Wilkinson (EW) model, in which the square of the surface width W^2 depends on time in logarithmic way. In Fig. 2(b), we find that the experimental data are also nicely fit to the prediction of EW model, $W^2 \sim \log t$.

The crossover behavior thus implies that the nonlinear effect such as the Kardar-Parisi-Zhang (KPZ) term, which
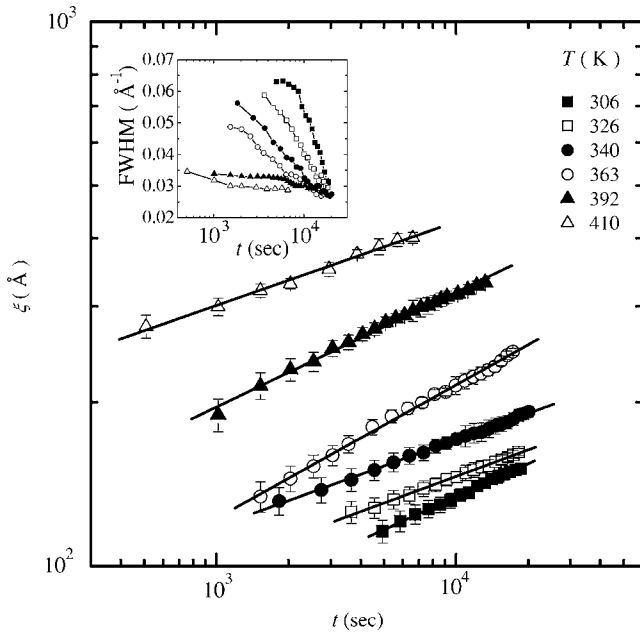
FIG. 6. Lateral characteristic length ξ as a function of sputtering time t for different substrate temperatures (symbols) with ϵ $=0.5$ keV and $f=0.5 \times 10^{13}$ ions/cm^2/s. Solid lines represent the curves best fit by the power law $\xi(t) \sim t^{1/z}$. Inset: FWHM of the satellite peaks as a function of sputtering time t for different T's.

FIG. 8. Evolution of the local slope m of the mounds or pits as a function of sputtering time t with $\epsilon=0.5$ keV and $f=0.5 \times 10^{13}$.

manifests itself in the form of large β values, disappears for $t > t_c$. This case can happen under two circumstances. (i) The erosion rate by sputtering is almost the same as the redeposition rate, and then the net erosion rate vanishes. (ii) When atoms are added onto surface, the downhill current of them is dominant, and thus roughening is not effective.

Recently, Tok, Ong, and Kang[24] has performed a kinetic Monte Carlo simulation for the evolution of sputter-eroded surface on the basis of the Sigmund theory. They also find that $W(t)$ exhibits a crossover similar to what we observe in the experiment. That is the crossover behavior to the EW scaling in the long time limit. In their model, the EW behav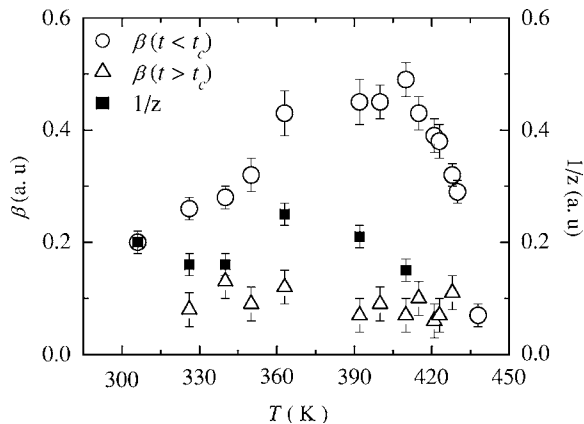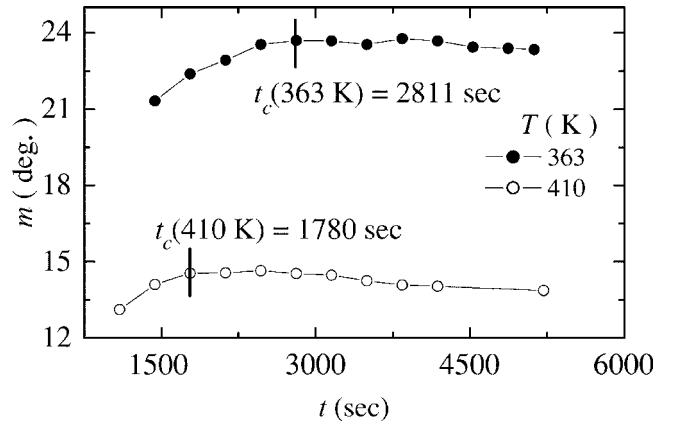ior mainly results from the balance between the erosion due to the external ion bombardment and the redeposition of sputtered atoms onto the surface. As sputtering proceeds, the surface becomes rough, and then the sputtered atoms have more chance to be captured at the hill than in the case where the surface is flat. Thus, as the surface becomes rougher, the balance can be more likely met. One may doubt this case because the redeposition rate is usually known as being far below 100%.[25] However, the apparent volume of vacancy island generated by ion impact is usually smaller than the mass actually removed, since the vacancy island exposed to vacuum likely encloses vacancies beneath it.[26] If the apparent volume of vacancy island and the redeposited volume are balanced, then the nonlinear term such as the KPZ term vanishes, and the surface is reduced to the EW scaling.

On the other hand, as the sputtering proceeds, the slope of the surface becomes steeper or the terrace width becomes narrower. Then, the ion-induced diffusion across step edge occurs more frequently, and strong downhill current can arise. Such a mechanism would also can be operative in the long time limit, and contribute to the EW scaling behavior.

It is still a nontrivial task to identify the atomistic mechanism for the crossover at t_c observed in the experiment. However, we note an interesting experimental result that t_c is almost coincident with the one when slope selection is initiated as shown in Fig. 8. Until t_c, the slope increases, and so does the blocking angle of the hill and the redeposited mass as a result. We speculate that the t_c signals the time when the slope of islands reach such a critical value that the redeposited mass is now balanced with the apparently removed mass. After then, morphological evolution is made just under the mass redistribution mechanism and the morphological evolution of the surafce is well described by a linear model, the Edwards-Wilkinson model.

FIG. 7. The temperature dependence of the growth exponent β before t_c and coarsening exponent $1/z$. The coarsening exponent $1/z$ shows weak temperature dependence compared with β before t_c.

B. General structural features of sputtered Pd(001) before t_c

One of the general features of the sputtered Pd(001) is the reentrant behavior in both $W(T)$ at fixed fluence and β: below $T_m \approx 410$ K, they slowly increase, but above T_m, they decrease steeply as shown in Figs. 3 and 7, respectively. The other characteristic morphological feature is that no slope selection is made over the whole temperature range before t_c:

coarsening develops less rapidly than roughening, $1/z$ being always smaller than β. For many sputtering and deposition events, however, slope selection has been predicted and observed.[19,27,28]

Both the abovementioned features are well reproduced in a simulation for MBE growth. Amar and Family[29] predict such an increase in β with increasing $T(<T_m)$ in their kinetic Monte Carlo (KMC) simulations for MBE growth. They attributed such results to the enhanced diffusivity of adatoms with increasing T: the more adatoms reach step edges, the larger is the destabilizing uphill current.[29] It is also noteworthy that Zhang, Detch, and Metiu[30] predict that if the step edge barrier is so effective that a total reflection is made at the edge, then β becomes 0.5 which is the largest value found for the present system near 410 K, implying that near 410 K, the Ehrlich-Schwöbel (ES) barrier is so effective that the total reflection of adatoms occurs at step edges. As temperature increases, however, reflectivity of adatoms at step edges should be diminished by $1-\exp[-(E_d+E_{ES})/kT]$, where E_d and E_{ES} are the diffusion barrier of adatoms over the terrace and the ES barrier at the step edge, respectively. The apparent total reflection near 410 K may reflect the contribution of reflected vacancies which become highly populated and mobile as T increases and compensates for the decreased reflectivity of adatoms.

It would be interesting to recall that an atomistic model in line with the above picture has been proposed by Ling *et al.*[31] The model suggests that the temperature dependence of the sputtered surface width W is determined mainly by the so-called ES diffusivity S that is proportional to the recoiling diffusivity as well as the step climbing probability and terrace diffusivity, defined as $S \propto (1-e^{-E_{ES}/kT})e^{-(E_0+E_1)/kT}$, where E_0 and E_1 are the barriers for step climbing and terrace diffusion, respectively. Actually, $S(T)$ shows a reentrant bell-shaped dependence on T; S rapidly grows when T is smaller than a certain temperature T_s where S is maximum, and very slowly decreases for $T>T_s$.

The temperature dependence of $S(T)$ is, however, in sharp contrast to the present and the other previous experimental results of $W(T)$ that show *slow* increase for $T<T_m$ and then *abrupt* drop for $T>T_m$. Hence, the observed dependence of W on temperature is not solely attributed to S of the adatom (or that of the vacancy). The model does not consider other important smoothing processes such as adatom detachment from the step edge, which is actually very efficient near T_m. (See Fig. 9 and the corresponding discussion in the following Sec. IV C.) Adatom detachment from step edges becomes more frequent as T increases, and should expedite the decrease of $W(T)$ for $T>T_m$. However, the relative amount of each contribution to the adatom current is not known, and thus our argument remains rather qualitative.

C. Comparison with models

As noticed from the above account, it is still a formidable task to have an atomistic picture for the morphological evolution of the sputtered surface. In this section, we will compare the predictions of various models with the present ex-
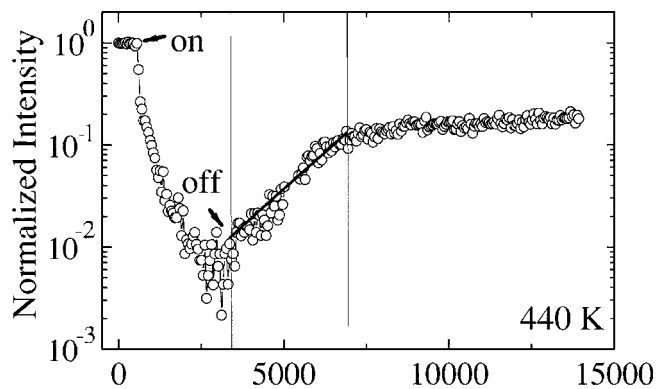

FIG. 9. Recovery of specular anti-Bragg intensity after sputtering a sample at 440 K with $\epsilon=0.5$ keV and $f=0.5\times10^{13}$ ions/cm^2/s. "on" signifies the start of sputtering and "off" the end of sputtering.

perimental results to obtain an insight into the most relevant microscopic mechanism of the roughening and coarsening kinetics.

Room temperature. For the systematic development of the present discussion, we first review our previous work on the sputtered morphology of Pd(001) at room temperature.[12] At 306 K, we find the sputtered surface consists of adatom islands rather than vacancy islands from an STM study of sputtered Pd(001). The adatom islands are not exactly square, and the edges of adatom islands are rather irregular. This indicates that the diffusion along the step edges of the islands is not sufficient to form compact islands with straight edges along the close-packed [110] direction at 306 K. In addition, W at fixed fluence is independent of the flux at room temperature, which indicates that effective diffusion is not thermally driven, but mainly ion induced.[32]

Both β and $1/z$ for $\varepsilon=0.5$ keV are 0.20 ± 0.02 at 306 K which is consistent with the formation of a facet on the sputtered surface observed in the GISAXS measurement. To explain such scaling behavior, we proposed a higher order correction to the Kuramoto-Sivashinsky (KS) model by adding a nonlinear term, the so-called conserved KPZ term $\lambda_2\nabla^2(\nabla h)^2$, where λ_2 is a tilt-dependent erosion rate and h is the surface height.[12]

High temperature regime, $T>410$ K. W decreases rapidly under constant fluence for $T>410$ K as shown in Fig. 3. β also decreases abruptly to 0.07 ± 0.02 at 440 K as in Fig. 7 after reaching a maximum value of 0.49 ± 0.04 at 410 K (Fig. 8). These facts indicate that a new diffusion process is activated for $T>410$ K that is very effective in smoothing the rough surface.

To identify the newly activated diffusion process above 410 K, we examine the recovery time of the specular anti-Bragg intensity after stopping sputtering at 440 K. Figure 9 shows that the anti-Bragg intensity recovers by $\sim10\%$ of its initial value. The activation energy barrier E_b is related to the relaxation time τ through the diffusivity $D=x^2/\pi^2a^2\tau$ $=A\exp(-E_b/kT)$, where $x=1000$ Å is the average terrace width, $a=2.75$ Å is the lattice constant of Pd(001), and A is the attempt frequency which is assumed to be 10^{12} s^{-1}.[14] τ is estimated by fitting $W(t)$ to $W_\infty[1-\exp(-t/\tau)]$ after stopping

TABLE I. Various activation energy barriers for atomic diffusion on the Pd(001) surface, excerpted from the results with effective medium theory by P. Stoltze (Ref. 33).

Diffusion of adatom along a step	0.308 eV
Diffusion of adatom on terrace	0.503 eV
Diffusion of vacancy on terrace	0.572 eV
ES barrier of adatom by hopping	0.573 eV
ES barrier of adatom by exchanging	0.698 eV
Detachment of adatom at step	0.922 eV

sputtering. W_∞ is the roughness in the long time limit. The E_b obtained from the above relation is 0.91 ± 0.05 eV. This value is close to the theoretical prediction for adatom detachment from steps, 0.922 eV (Table I).[33] It indicates that the step adatom detachment process becomes active for $T > 410$ K.

To smoothen the surface, overcoming the step edge barriers E_{ES} for both sputter-induced adatoms and vacancies is a critical process, because such a process reduces the destabilizing uphill (downhill) current of sputter-induced adatoms (vacancies) biased by ES barriers. Detachment of atoms from step edges is an important process for smoothing rough surfaces. This contributes to the uphill current of vacancies, because atom detachment from the step edge is necessary for vacancies to cross step edges. For Pt(111), Michely *et al.*[15] observed by STM study that atoms detached from step edges effectively anneal vacancy islands, resulting in a smooth surface. The contribution of the uphill current of vacancies to smoothing the rough surface increases as T increases, since the dominant surface species becomes vacancies rather than adatoms as observed in Ag(001) (Refs. 2 and 22) and Co(0001) (Ref. 14) due to the relatively high diffusion barriers for vacancies compared with those for adatoms (Table I).

Intermediate temperature regime, $306 \text{ K} < T < 410 \text{ K}$. For T around 350 K, we find that β is about 0.25, while $1/z$ is about 0.16 (Fig. 7). Amar and Family[29] obtained β and $1/z$ to be 0.24 and 0.18, respectively, under the condition of no slope selection through their KMC simulation for the MBE growth of Fe on a Fe(001) system. Such exponents are in good agreement with our experimental observation for T around 350 K. This means that the morphological evolution of the sputtered Pd(001) is well described by deposition and the diffusion processes of adatoms. It is also anticipated from the adatom dominant surface observed by STM for sputtered Pd(001) near 306 K.[12]

As T increases above 350 K but below 410 K, β increases rapidly to 0.45–0.5 and $1/z$ varies from 0.15 to 0.25 (Fig. 8). Amar and Family[29] also performed KMC simulations at a temperature elevated by 60 K. They find that β increases to be 0.45, while $1/z$ changes slightly to 0.16. The simulation result of β is in excellent agreement with the present experimental value, while the $1/z$ value shows a discrepancy by 0.1 at its maximum from the experimental value. Such a discrepancy may reflect the deviation of the sputtering process from MBE growth near T_m, or the contribution of vacancy to morphological evolution of sputtered Pd(001) at elevated temperatures.

Golubović[34] proposed a continuum model containing both a destabilizing surface current generated by the ES barrier and relaxation by surface diffusion with no slope selection. The model predicts $\beta = 0.50$ and $1/z = 0.25$ under the assumption that the Mullin's term $\nabla^4 h$ is the most relevant term for surface relaxation. However, if the higher order term, $\nabla^6 h$ is more relevant and $1/z$ is reduced to 0.16. In our experiment, β is around 0.45–0.5, while $1/z$ varies from 0.25 to 0.15 as T varies from 363 to 410 K. According to the model of Golubović, Mullin's term is the dominant surface relaxation term near 363 K, giving 0.25 for $1/z$. As T further increases to 410 K, surface relaxation is not governed by Mullin's term, but by the higher order term $\nabla^6 h$ resulting in a value of 0.16 for $1/z$. Further studies on the microscopic level are, however, awaited to examine our experimental results against the theoretical predictions.

D. Lateral ordering

The lateral ordering is observed for islands larger than at least 100 Å, as noticed from the first discernable satellite peak observed at each T in Fig. 6. Further, the ordering becomes better as the island size increases, because the full width at half maximum (FWHM) of the satellite peak monotonically decreases with increasing island size (inset of Fig. 6). The FWHM reflects the statistical size distribution of the lateral features and the degree of in-plane order in the position of the islands on the sputtered surface.[35] For all the experimental T, FWHM decreases with increasing sputter time t. (FWHMs converge at late times because the instrumental resolution limit is, 0.015 Å^{-1}.) Such an observation tells us that the lateral ordering and uniformity of the island size improves with increasing island size.

Studying the strain effect of islands on their self-organized pattern formation during MBE growth, Shchukin and Bimberg[36] find that the development of a well-ordered strain field and the ordering of islands are realized if the islands reach some critical size. In the present experiment, it is not clear whether there is any critical ξ where lateral order develops. However, it seems very probable that a sputter-induced, ordered strain field drives lateral ordering of sputtered features, in regards to the improvement of order and uniformity of surface features with increasing sputter time and island size ξ.

V. SUMMARY AND CONCLUSION

We have investigated the temperature dependence of both roughening and coarsening kinetics of Ar$^+$ sputtered Pd(001) employing *in situ*, real-time x-ray reflectivity and grazing-incidence small angle x-ray scattering. We obtained the surface roughness $W(t)$, the growth exponent β, as well as the coarsening exponent $1/z$. Both the W and β showed a bell-shaped, reentrant behavior. The observed scaling exponents are close to those predicted in the kinetic Monte Carlo simulation for the MBE growth under the condition of no slope selection, implying that the morphological evolution of the sputtered surface is largely described by deposition and diffusion processes.

When the temperature is increased, the roughness of the surface grows to a certain characteristic temperature T_m. Near T_m, we found noticeable discrepancy between the KMC simulation and the experimental results. In such a high temperature regime, processes other than the adatom deposition and diffusion, e.g., vacancy diffusion and adatom detachment from the step edges seem to contribute to the formation of surface morphology, especially the smoothing.

*Author to whom correspondence should be addressed. Electronic address: jskim@sookmyung.ac.kr

[1] S. Facsco, T. Dekorsy, C. Koerdt, C. Trappe, H. Kurz, A. Vogt, and H. L. Hartnagel, Science **285**, 1551 (1999).

[2] G. Costantini, S. Rusponi, R. Gianotti, C. Boragno, and U. Valbusa, Surf. Sci. **416**, 245 (1998).

[3] S. Rusponi, C. Boragno, and U. Valbusa, Phys. Rev. Lett. **78**, 2795 (1997).

[4] S. Rusponi, G. Costantini, C. Boragno, and U. Valbusa, Phys. Rev. Lett. **81**, 2735 (1998).

[5] J. C. Girard, Y. Samson, S. Gautier, S. Rousset, and J. Klein, Surf. Sci. **302**, 73 (1994).

[6] J. Naumann, J. Osing, A. J. Quinn, and I. V. Shverts, Surf. Sci. **388**, 212 (1997).

[7] R. M. Bradley and J. M. E. Harper, J. Vac. Sci. Technol. A **6**, 2390 (1988).

[8] A.-L. Barabási and H. E. Stanley, *Fractal Concepts in Surface Growth* (Cambridge University Press, Cambridge, 1995).

[9] Y. Kuramoto, *Chemical Oscillations, Waves and Turbulence* (Springer, Berlin, 1984); G. I. Sivashinsky and D. M. Michelson, Prog. Theor. Phys. **63**, 2112 (1980).

[10] R. Cuerno and A.-L. Barabási, Phys. Rev. Lett. **74**, 4746 (1995).

[11] S. Park, B. Kahng, H. Jeong, and A.-L. Barabási, Phys. Rev. Lett. **83**, 3486 (1999).

[12] T. C. Kim, C.-M. Ghim, H. J. Kim, D. H. Kim, D. Y. Noh, N. D. Kim, J. W. Chung, J. S. Yang, Y. J. Chang, T. W. Noh, B. Kahng, and J.-S. Kim, Phys. Rev. Lett. **92**, 246104 (2004).

[13] M. Castro, R. Cuerno, L. Vázquez, and R. Gago, Phys. Rev. Lett. **94**, 016102 (2005).

[14] O. Malis, J. D. Brock, R. L. Headrick, M.-S. Yi, and J. M. Pomeroy, Phys. Rev. B **66**, 035408 (2002).

[15] T. Michely, M. Kalff, G. Comsa, M. Strobel, and K.-H. Heinig, Phys. Rev. Lett. **86**, 2589 (2001).

[16] I. Koponen, M. Hautala, and O.-P. Sievänen, Phys. Rev. Lett. **78**, 2612 (1997).

[17] G. Costantini, S. Rusponi, F. B. de Mongeot, C. Borango, and U. Valbusa, J. Phys.: Condens. Matter **13**, 5875 (2001).

[18] M. V. Ramana Murty, T. Curcic, A. Judy, B. H. Cooper, A. R. Woll, J. D. Brock, S. Kycia, and R. L. Headrick, Phys. Rev. B **60**, 16 956 (1999); M. V. R. Murty, B. Cowels, and B. H. Cooper, Surf. Sci. **415**, 328 (1998).

[19] M. V. Ramana Murty, T. Curcic, A. Judy, B. H. Cooper, A. R. Woll, J. D. Brock, S. Kycia, and R. L. Headrick, Phys. Rev. Lett. **80**, 4713 (1998).

[20] S. K. Sinha, E. B. Sirota, S. Garoff, and H. B. Stanley, Phys. Rev. B **38**, 2297 (1988).

[21] L. G. Parratt, Phys. Rev. **95**, 359 (1954).

[22] G. Costantini, F. Buatier de Mongeot, C. Boragno, and U. Valbusa, Phys. Rev. Lett. **86**, 838 (2001).

[23] The characteristic length ξ reflects the average spacing between the islands. Since the islands are more or less packed compactly, that is, islands are almost touching each other as shown by STM image in our previous work (Ref. 12), ξ is probably proportional to the island size, and taken as a measure for the island size.

[24] E. S. Tok, S. W. Ong, and H. C. Kang, Phys. Rev. E **70**, 011604 (2004).

[25] T. Michely and C. Teichert, Phys. Rev. B **50**, 11 156 (1994).

[26] C. Busse, H. Hansen, U. Linke, and T. Michely, Phys. Rev. Lett. **85**, 326 (2000).

[27] J. A. Stroscio, D. T. Pierce, M. D. Stiles, A. Zangwill, and L. M. Sander, Phys. Rev. Lett. **75**, 4246 (1995).

[28] M. Siegert and M. Plischke, Phys. Rev. Lett. **73**, 1517 (1994).

[29] J. G. Amar and F. Family, Phys. Rev. B **54**, 14 742 (1996).

[30] Z. Zhang, J. Detch, and H. Metiu, Phys. Rev. B **48**, R4972 (1993).

[31] L. Ling, W. Q. Li, L. J. Qi, M. Lu, X. Yang, and C. X. Gu, Phys. Rev. B **71**, 155329 (2005).

[32] M. A. Makeev and A.-L. Barabási, Appl. Phys. Lett. **71**, 2800 (1997).

[33] P. Stoltze, J. Phys.: Condens. Matter **6**, 9495 (1994).

[34] L. Golubobić, Phys. Rev. Lett. **78**, 90 (1997).

[35] The FWHM depends on the islands size since it is related to the average distance between the islands. We note, however, that the FWHM decreases by more than factor of two except for the data at 392 and 410 K data, while ξ increases less than factor of two. Therefore, we might claim that the positional ordering or uniformity increases as the islands become larger.

[36] V. A. Shchukin and D. Bimberg, Rev. Mod. Phys. **71**, 1125 (1999).